J|A|C|S
ARTICLES
Published on Web 04/16/2003

Axial Solvent Coordination in "Base-Off" Cob(II)alamin and Related Co(II)-Corrinates Revealed by 2D-EPR

Sabine Van Doorslaer,[†,⊥] Gunnar Jeschke,[‡] Boris Epel,[§] Daniella Goldfarb,[§] Rüdiger-Albert Eichel,[†,#] Bernhard Kräutler,[∥] and Arthur Schweiger*[,†]

Contribution from the Laboratory of Physical Chemistry, ETH Hönggerberg, CH-8093 Zurich, Switzerland, Max-Planck-Institut für Polymerforschung, Postfach 3148, D-55021 Mainz, Germany, The Weizmann Institute of Science, Rehovot, 76100, Israel, and Institute for Organic Chemistry, University of Innsbruck, A-6020 Innsbruck, Austria

Received September 27, 2002; E-mail: schweiger@esr.phys.chem.ethz.ch.

Abstract: Detailed information on the structure of cobalt(II) corrinates is of interest in the context of studies on the coenzyme B_{12} catalyzed enzymatic reactions, where cob(II)alamin has been identified as a reaction intermediate. Cob(II)ester (heptamethyl cobyrinate perchlorate) is found to be soluble in both polar and nonpolar solvents and is therefore very suitable to study solvent effects on Co(II) corrinates. In the literature, Co(II) corrinates in solution are often addressed as four-coordinated Co(II) corrins. However, using a combination of continuous-wave (CW) and pulse electron paramagnetic resonance (EPR) and pulse ENDOR (electron nuclear double resonance) at different microwave frequencies we clearly prove axial ligation for Cob(II)ester and the *base-off* form of cob(II)alamin (B_{12r}) in different solvents. This goal is achieved by the analysis of the *g* values, and the hyperfine couplings of cobalt, some corrin nitrogens and hydrogens, and solvent protons. These parameters are shown to be very sensitive to changes in the solvent ligation. Density functional computations (DFT) facilitate largely the interpretation of the EPR data. In the CW-EPR spectrum of Cob(II)ester in methanol, a second component appears below 100 K. Different cooling experiments suggest that this observation is related to the phase transition of methanol from the α-phase to the glassy state. A detailed analysis of the EPR parameters indicates that this transition induces a change from a five-coordinated (above 100 K) to a six-coordinated (below 100 K) Co(II) corrin. In a CH_3OH:H_2O mixture the phase-transition properties alter and only the five-coordinated form is detected for Cob(II)ester and for *base-off* B_{12r} at all temperatures. Our study thus shows that the characteristics of the solvent can have a large influence on the structure of Co(II) corrinates and that comparison with the protein-embedded cofactor requires some caution. Finally, the spectral similarities between Cob(II)ester and *base-off* B_{12r} prove the analogies in their electronic structure.

Introduction

More than 50 years after the first isolation of the red cobalt complex B_{12} as the (extrinsic) anti-pernicious anaemia factor,[1,2] B_{12} and B_{12}-proteins are still the subject of a vast amount of interdisciplinary studies.[3,4] As a rule, B_{12} derivatives are involved in unique organo-metallic biological reactions. Frequently, cobalt(II) corrins such as cob(II)alamin (B_{12r}) are relevant intermediates in such enzymatic processes but are formed transiently and are difficult to observe. When the formal oxidation state of the cobalt atom decreases, its coordination number tends to decrease correspondingly. In the thermodynamically predominating forms, the coordination number is generally believed to be 6 (two axial ligands) for Co^{III}, 5 (one axial ligand) for Co^{II}, and 4 (no axial ligand) for Co^{I}. Cob(II)-alamin complexes in which the dimethylbenzimidazole (DBI) group is coordinated to the cobalt atom are named *base-on* forms, whereas if such a coordination is absent or replaced by an exogeneous ligand these complexes are designated as *base-off* complexes. In crystals of Co^{II} corrins external axial ligands have been found to coordinate at the less hindered β-face of the Co^{II} center,[5,6] whereas in B_{12r} the nucleotide base is intramolecularly directed to the α-face of the Co^{II} center.[7]

The *base-on* form represents the most stable constitution of the isolated B_{12} cofactors in solution at neutral pH and in the

[†] Laboratory of Physical Chemistry, ETH Hönggerberg.
[‡] Max-Planck-Institut für Polymerforschung.
[§] The Weizmann Institute of Science.
[∥] Institute for Organic Chemistry, University of Innsbruck.
[⊥] Current address: SIBAC Laboratory, Department of Physics, University of Antwerp, B-2610 Wilrijk, Belgium.
[#] Current address: Institute for Physical Chemistry, Darmstadt University of Technology, D-64287 Darmstadt, Germany.

(1) Rickes, E. L.; Brink, N. G.; Koniuszy, F. R.; Wood, T. R.; Folkers, K. *Science* **1948**, *107*, 396−397.
(2) Smith, E. L.; Parker, F. *J. Biochem.* **1948**, *43*, VIII.
(3) Kräutler, B., Arigoni, D., Golding, B. T. Eds. *Vitamin B_{12} and B_{12}-Proteins*.; Wiley-VCH: Weinheim, 1998.
(4) Banerjee, R., Ed. *Chemistry and Biochemistry of B_{12}*; J. Wiley & Sons: New York, 1999.
(5) (a) Glusker, J. P. In *B_{12}*; Dolphin, D., Ed.; John Wiley & Sons: New York, Chichester, 1982; Vol. I, p 23. (b) Rossi, M.; Glusker, J. P. In *Molecular Structure and Energetics*; Liebman, J. F., Greenberg, A., Eds.; VCH Publishers: Weinheim, (FRG), 1988; Vol. X, p 1.
(6) Kräutler, B.; Keller, W.; Hughes, M.; Caderas, C.; Kratky, C. *J. Chem. Soc., Chem. Commun.* **1987**, 1678−1680.
(7) Kräutler, B.; Keller, W.; Kratky, C. *J. Am. Chem. Soc.* **1989**, *111*, 8936−8938.

solid state.[3,4] The crystal structure of the B_{12}-binding domain of methionine synthase (MetH) from *Escherichia coli* revealed a surprisingly different situation for the protein-bound methylcob(III)alamin. Instead of the intramolecular DBI base, the imidazole side chain of the protein residue His759 was found to coordinate at the corrin-bound Co^{III} center (the *base-off*/*His-on* constitution).[8−10] This constitution was also found in methylmalonyl-CoA mutase (MCM) from *Propionibacterium shermanii*[10,11] and for glutamate mutase (Glm) from *Clostidium cochlearium*.[12] Contrasting these findings, EPR-spectroscopic studies and X-ray studies on the mode of binding of coenzyme B_{12} to diol dehydratase (DD) and to B_{12}-dependent ribonucleotide reductase (RNR) indicated *base-on* binding of the corrinoid cofactor.[13−17] Furthermore, it was reported that 5-methoxybenzimidazolylcobamide and 5-hydroxybenzimidazolycobamide in the corrinoid/iron−sulfur proteins from *Clostridium thermoaceticum*[18] and *Methanosarcina thermophila*,[19] respectively, lack histidine ligation although their benzimidazole bases are uncoordinated to the cobalt atom (*base-off*).

Studies concerning the axial coordination properties of cobalt-corrinates are therefore of interest, as the homolytic and heterolytic organometallic reactivity of these systems are central to their biological role. Recent indications that the Co-coordinated histidine in MetH helps to control the organometallic reactivity of the protein-bound corrinoid[8−10] and the observation that the axial Co−N bond in MCM, Glm and DD is unusually long[11,12,15] have given even more relevance to such investigations. There is still some discussion on the coordination number of the *base-off* form of free B_{12r}. Lexa and Saveant proposed two possible structures for electrochemically produced B_{12r}: pentacoordinate *base-off* (water ligation) and pentacoordinate *base-on* (DBI ligation) below and above pH 2.9, respectively.[20] Giorgetti et al. showed using EXAFS and XANES that basically a pentacoordinated Co^{II} form is formed at low pH with a long axial bond to oxygen (0.222 nm).[21] A time-resolved XAS of the photoreduced *base-off* cob(II)alamin suggested the formation of a four-coordinated Co^{II} form which persists for 5 ns to 10 ms.[22] The same study indicated that the chemically induced free *base-off* B_{12r} is six-coordinated with strong ligation to water.

The transient intermediate cob(II)alamin and related Co^{II} corrin systems can very nicely be studied by EPR and ENDOR (electron nuclear double resonance).[4,18,23,24] In the past two decennia, a large number of pulse EPR and ENDOR techniques have been developed which help to reveal detailed structural and electronic information on paramagnetic systems.[25]

In this work, we compare the electronic and structural properties of protonated *base-off* B_{12r} ($\mathbf{2}^+H_2PO_4^-$) in a methanol:water solution with those of heptamethyl cobyrinate perchlorate[6,26] ([Cob(II)ester]ClO_4, $\mathbf{1}^+ClO_4^-$) in different solvents. [Cob(II)ester]ClO_4 has the relevant structural features of *base-off* B_{12r}, because the corrin ligand of $\mathbf{1}^+$ is derived directly from B_{12}. It differs from the structure of *base-off* B_{12r} in the periphery only, where the six carboxamide substituents and the characteristic nucleotide function of *base-off* B_{12r} are replaced by methyl ester groups (see Scheme 1). Because $\mathbf{1}^+ClO_4^-$ can be dissolved in both apolar and polar solvents, it is an ideal model system to study the effects of axial coordination of solvent molecules on the electronic and structural characteristics of Co^{II} corrins. Apart from acting as model systems for B_{12} derivatives, it is interesting to note that aquacyanocobalt(III)-cobyrinate derivatives (related to $\mathbf{1}^+ClO_4^-$) are being used in NO_2-selective fire-detection systems.[27]

In this work, we show that the use of continuous wave (CW) EPR spectroscopy at X-band frequencies (ca. 9 GHz) and pulse-EPR and ENDOR techniques at X-, Q- and W-band frequencies (9, 35 and 95 GHz) reveals interesting information on the solvent-binding properties of $\mathbf{1}^+$ and $\mathbf{2}^+$. For the first time, clear evidence of axial solvent ligation in *base-off* Co(II) corrinates is shown. The data interpretation could be corroborated using density functional (DFT) calculations. The present findings can have important consequences for the analysis of B_{12r} protein data, where the lack of a nitrogen coupling is sometimes interpreted in terms of the presence of four-coordinate Co(II) corrin.[3,4,18] Furthermore, an interesting behavior related to phase transitions in the solvent was detected for $\mathbf{1}^+$ in methanol. This observation prompts for caution when extrapolating data on model systems to the cofactor in the protein. Finally, the suitability of $\mathbf{1}^+$ as a model system for $\mathbf{2}^+$ could be proven.

This work is part of a larger investigation on the axial ligation and oxygenation properties of Co^{II} corrin systems[28−32] in comparison to Co^{II} porphyrin complexes.[33−36] These studies are

(8) Drennan, C. L.; Huang, S.; Drummond, J. T.; Matthews, R. G.; Ludwig, M. L. *Science* **1994**, *266*, 1669−1674.
(9) Ludwig, M. L.; Drennan, C. L.; Matthews, R. G. *Structure* **1996**, *4*, 505−512.
(10) Ludwig, M. L.; Evans, P. R. In ref 4, pp 595−632.
(11) Mancia, F.; Keep, N. H.; Nakagawa, A.; Leadlay, P. F.; McSweeney, S.; Rasmussen, B.; Bosecke, P.; Diat, O.; Evans, P. R. *Structure*, **1996**, *4*, 339−350.
(12) Reitzer, R.; Gruber, K.; Jogl, G.; Wagner, U. G.; Bothe, H.; Buckel, W.; Kratky, C. *Structure Fold. Des.* **1999**, *7*, 891−902.
(13) Abend, A.; Nitsche, R.; Bandarian, V.; Stupperich, E.; Retey, J. *Angew. Chem., Int. Ed.* **1998**, *37*, 625−627.
(14) Yamanishi, M.; Yamada, S.; Muguruma, H.; Murakami, Y.; Tobimatsu, T.: Ishida, A.; Yamauchi, J.; Toraya, T. *Biochemistry* **1998**, *37*, 4799−4803.
(15) Lawrence, C. C.; Gerfen, G. J.; Samano, V.; Nitsche, R.; Robins, M. J.; Retey, J.; Stubbe, J. *J. Biol. Chem.* **1999**, *274*, 7039−7042.
(16) Shibata, N.; Masuda, J.; Tobimatsu, T.; Toraya, T.; Suto, K.; Morimoto, Y.; Yasuoka, N. *Structure* **1999**, *7*, 997−1008.
(17) Sintchak, M. D.; Arjara, G.; Kellogg, B. A.; Stubbe, J.; Drennan, C. L. *Nature Structure Biology* **2002**, *9*, 293−300.
(18) Wirt, M. D.; Kumar, M.; Ragsdale, S. W.; Chance, M. R. *J. Am. Chem. Soc.* **1993,** *115*, 2146−2150.
(19) Jablonski, P. E.; Lu, W.-P.; Ragsdale, S. W.; Ferry, J. G. *J. Biol. Chem.* **1993**, *268*, 325−329.
(20) Lexa, D.; Saveant, J.-M. *Acc. Chem. Res.* **1983**, *16*, 235−243.
(21) Giorgetti, M.; Ascone, I.; Berrettoni, M.; Conti, P.; Zamponi, S.; Marassi, R. *JBIC* **2000**, *5*, 156−166.
(22) Scheuring, E. M.; Clavin, W.; Wirt, M. D.; Miller, L. M.; Fischetti, Y. L.; Mahoney, N.; Xie, A.; Wu, J.; Chance, M. R. *J. Phys. Chem.* **1996**, *100*, 3344−3348.
(23) Pilbrow, J. R. In *B12*; John Wiley & Sons: New York, Chichester, 1982; Vol. X, Vol. I, pp 431−462.
(24) Trommel, J. S.; Warncke, K.; Marzilli, L. G. *J. Am. Chem. Soc.* **2001**, *123*, 3358−3366.
(25) Schweiger, A.; Jeschke, G. *Principles of Pulse Electron Paramagnetic Resonance*; Oxford University Press: Oxford 2001.
(26) Murakami, Y.; Hisaeda, Y.; Kajihara, A. *Bull. Chem. Soc. Jpn.* **1983**, *56*, 3642−3646.
(27) Nezel, T.; Spichiger-Keller, U.; Ludin, C.; Hensel, A. *Chimia* **2001**, *55*, 725−731.
(28) Jörin, E.; Schweiger, A.; Günthard Hs. H. *Chem. Phys. Lett.* **1979**, *61*, 228−232.
(29) Jörin, E.; Graf, F.; Schweiger, A.; Günthard Hs. H. *Chem. Phys. Lett.* **1976**, *42*, 376−379.
(30) Jörin, E.; Schweiger, A.; Günthard Hs. H. *J. Am. Chem. Soc.* **1983**, *105*, 4227−4286.
(31) Van Doorslaer, S.; Kräutler, B.; Schweiger, A. *J. Phys. Chem. B* **2001**, *105*, 7554−7563.
(32) Harmer, J.; Van Doorslaer, S.; Gromov, I.; Schweiger, A. *Chem. Phys. Lett.* **2002**, *358*, 8−16.
(33) Van Doorslaer, S.; Bachmann, R.; Schweiger, A. *J. Phys. Chem. A* **1999**, *103*, 5446−5455.
(34) Van Doorslaer, S.; Schweiger, A. *J. Phys. Chem. B* **2000**, *104*, 2919−2927.

Scheme 1. Structures of [Cob(II)Ester]ClO_4 ($1^+ClO_4^-$), *Base-Off* B_{12r} ($2^+H_2PO_4^-$) and Co^{II} Corrin (3^+)[a]

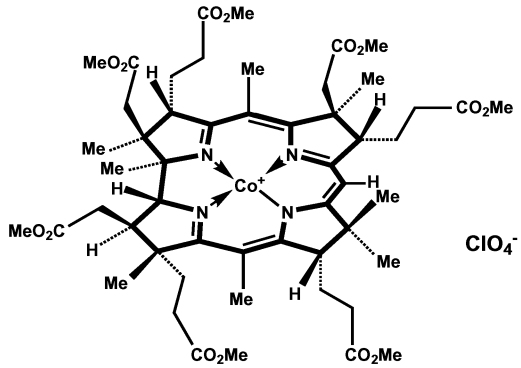

($1^+ClO_4^-$)

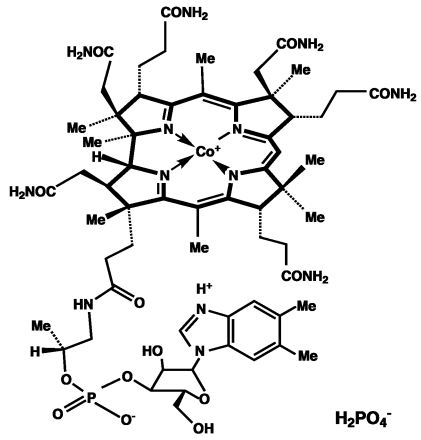

($2^+H_2PO_4^-$)

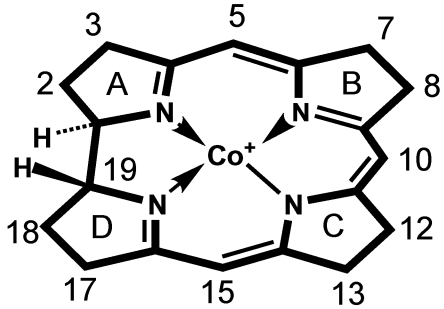

(3^+)

[a] The structures are shown without their possible axial ligands which are solvent dependent

aimed at the evaluation of the specific bonding characteristics of the unique corrin ligand in comparison to the more symmetric and more "common" porphyrin ligand.

Experimental Procedures

Sample Preparation. Heptamethyl cobyrinate perchlorate, [Cob(II)ester]ClO_4 ($1^+ClO_4^-$), was prepared as described in ref 6. As solvents, purified absolute toluene, methanol, CH_2Cl_2 and water (all from Fluka) were used. Toluene, methanol, and CH_2Cl_2 were additionally dried by condensation onto 3 Å molecular sieves (Fluka) under vacuum as described in refs 37 and 38. Deuterated toluene-d_8 (>99.6% purity), methanol-d_4 (> 99.96% purity), and methanol-d_3 (> 99% purity) were obtained from Cambridge Isotope Laboratories (CIL). [Cob(II)ester]ClO_4 was dissolved in toluene, in methanol, in a 1:1 methanol−water mixture and in CH_2Cl_2 to a final concentration of 2×10^{-3} M (glovebox, N_2 atmosphere (<1 ppm O_2)). After mixing of the components, the solutions were transferred to the X-band and Q-band EPR tubes and evacuated at a vacuum line using the usual freeze−pump−thaw method. During all procedures, O_2 was excluded to prevent formation of the oxygenated complexes. For the preparation of the W-band samples, a slightly different approach had to be used. After being filled under N_2 atmosphere, the quartz tubes (0.5 mm inner diameter) were sealed with wax and removed from the glovebox. They were then centrifuged for 30 s and immediately afterwards sealed by melting the quartz.

Hydroxocob(III)alamin hydrochloride (B_{12a}) was purchased from Fluka. All solvents and liquid reagents were degassed prior to use. All procedures were carried out in a glovebox under N_2 atmosphere (<1 ppm O_2) to prevent oxidation of the final product. Hydroxocob(III)alamin was reduced using the method described by Tollinger et al.[39] A 1000 mg portion of hydroxocob(III)alamin hydrochloride was dissolved in 20 mL of water, after which a 0.5 mL portion of formic acid and 1.85 mL of triethylamine were added. The reduction to cob(II)alamin, B_{12r}, could be monitored visually (change of deep red to brown color). Subsequently, B_{12r} was precipitated out of the solution by addition of acetone. After filtration and washing, B_{12r} was dissolved in a 1:1 methanol:water mixture (final B_{12r} concentration: $5\ 10^{-3}$ M). H_3PO_4 was used to bring the solution to a final pH of 1.4 in order to form the *base-off* B_{12r} form $2^+H_2PO_4^-$ (pK_a ($2^+H_2PO_4^-$) = 2.9 [20]). The solution was transferred to an EPR tube and degassed on a vacuum line using the freeze−pump−thaw method.

Spectroscopy. Continuous Wave EPR Spectroscopy. The X-band CW-EPR spectra were recorded on a Bruker ESP300 spectrometer (microwave (mw) frequency, 9.43 GHz) equipped with a liquid helium cryostat from Oxford Inc. The magnetic field was measured using a Bruker ER035M NMR Gaussmeter. An mw power of 20 mW, a modulation amplitude of 0.5 mT and a modulation frequency of 100 kHz were used. Simulations were done using the XSophe program of Bruker.

Pulse EPR Spectroscopy. The X-band Electron-Zeeman (EZ)[40,41] resolved EPR spectra were recorded on a home-built X-band pulse EPR spectrometer (9.15 GHz)[42] with a home-built dielectric ring resonator.[43] The experiment was carried out using the mw three-pulse sequence, $\pi/2$-τ-$\pi/2$-T-$\pi/2$-τ-*echo*, with pulse lengths $t_{\pi/2} = 50$ ns for the first two pulses and $t_{\pi/2} = 20$ ns for the last pulse. Time intervals $\tau = 360$ ns and $T = 6.2$ μs and a field modulation frequency $\nu_{ez} = 64$ kHz were used. The setup for the field modulation consists of an arbitrary function generator (AFG, LeCroy 9100), a radio frequency amplifier (AR 100A500A) and a Helmholtz coil for the field modulation. The experiment was carried out with a repetition rate of 250 Hz.

The other X-band pulse EPR and ENDOR spectra (15 K throughout) were recorded on a Bruker Elexsys spectrometer (mw frequency 9.71 GHz) equipped with a liquid helium cryostat from Oxford Inc. The magnetic field was measured with a Bruker ER 035M NMR gaussmeter. In all pulse EPR experiments, a repetition rate of 1 kHz was used.

The Q-band pulse EPR spectra (15 K throughout) were recorded on a home-built spectrometer (mw frequency 35.28 GHz) equipped with

(35) Van Doorslaer, S.; Schweiger, A. *Phys. Chem. Chem. Phys*. **2001**, *3*, 159−166.
(36) Van Doorslaer, S.; Zingg, A.; Schweiger, A.; Diederich, F. *Chem. Phys. Chem*. **2002**, *3*, 659−667.
(37) Burfield, D. R.; Smithers, R. H. *J. Org. Chem*. **1983**, *48*, 2420−2422.
(38) Burfield, D. R.; Gan, G.-H.; Smithers, R. H. *J. Appl. Chem. Biotechnol*. **1978**, *28*, 23−30.
(39) Tollinger, M.; D'erer, T.; Konrat, R.; Kräutler, B. *J. Mol. Catal. A: Chem*. **1997**, *116*, 147−155.
(40) Eichel, R.-A.; Schweiger, A. *J. Magn. Reson*. **2001**, *152*, 276−287.
(41) Eichel, R.-A.; Schweiger, A. *Chem. Phys. Lett*. **2002**, *358*, 271−277.
(42) Wacker, T. Ph.D. Thesis No. 9913, ETH Zürich, 1992.
(43) Sierra, G. A., Ph.D. Thesis No. 1224, ETH Zürich, 1997.

a Bruker ENDOR ER5106 QTE probehead and an Oxford liquid Helium cryostat.[44] In all experiments, a repetition rate of 200 Hz was used.

W-band pulse EPR and ENDOR measurements were carried out at 94.9 GHz and 4.5 K using a home-built spectrometer described elsewhere.[45] The magnetic field values were calibrated using the Larmor frequency of the protons, ν_H, as determined by the ENDOR measurements.

HYSCORE (Hyperfine Sublevel Correlation):[46] The X-band experiments were carried out with the pulse sequence $\pi/2$-τ-$\pi/2$-t_1-π-t_2-$\pi/2$-τ-*echo* with pulse lengths $t_{\pi/2} = 24$ ns and $t_\pi = 16$ ns. The time intervals t_1 and t_2 were varied from 96 to 6400 ns in steps of 16 ns. A value of 96 ns was taken for τ. An eight-step phase cycle was used to eliminate unwanted echoes. The time traces of the HYSCORE spectra were baseline corrected with a third-order polynomial, apodized with a Hamming window and zero filled. After two-dimensional Fourier transformation, the absolute-value spectra were calculated. The HYSCORE spectra were simulated using the TRYSCORE program[47] and using an in-house written program.[48] Both simulation procedures led to basically the same results.

Electron Spin−Echo (ESE)-Detected EPR: The experiment was carried out at Q-band with the pulse sequence $\pi/2$-τ-π-τ-*echo* with pulse lengths $t_{\pi/2} = 50$ ns and $t_\pi = 100$ ns and $\tau = 550$ ns. The intensity of the primary echo was observed as a function of the magnetic field.

Davies-ENDOR:[49] The spectra were measured at X-band (W-band) with the sequence π-T-$\pi/2$-τ-π-τ-*echo*, with mw pulse lengths of $t_{\pi/2} = 50$ (100) ns, $t_\pi = 100$ (200) ns, and time intervals $\tau = 350$ (400) ns and $T = 13.5$ (20) μs. A radio frequency π pulse of variable frequency ν_{rf} and length 12 (14) μs was applied during time T.

Mims-ENDOR:[50] The W-band ^{2}H-ENDOR spectra were measured with the sequence $\pi/2$-τ-$\pi/2$-T-$\pi/2$-τ-*echo*, with mw pulse lengths of $t_{\pi/2} = 50$ ns and time intervals $\tau = 200$ ns and $T = 20$ μs. A radio frequency π pulse of variable frequency ν_{rf} and length 14 μs was applied during time T. A repetition rate of 100 Hz was used.

The ENDOR spectra were simulated using the MATLAB-based program EasySpin developed at the Laboratory of Physical Chemistry ETH Zurich (http://www.esr.ethz.ch).

DFT Computations. Spin-unrestricted density functional computations of hyperfine and nuclear quadrupole couplings were performed with the Amsterdam Density Functional (ADF 2000.01) package.[51−54] The geometry optimizations were done using the BLYP functional together with a Slater-type basis set of triple-ζ quality and a single set of polarization functions (basis set IV). For the computation of the hyperfine and nuclear quadrupole parameters in ADF, we used the BLYP functional and a triple-ζ basis set with double polarization functions with the zeroth-order relativistic approximation (basis set ZORA V).[55] The initial guess for the self-consistent field iteration was provided by the result of a single-point computation with a double-ζ basis set without polarization functions (ZORA II) to improve the convergence behavior with the larger basis set. Nuclear quadrupole moments for the computation of the nuclear quadrupole tensors from the electric field gradients were taken from ref 56. Data analysis and visualization were performed with a home-written program based on Matlab (The Math Works, Inc.). For the **g** tensor computations, we applied the spin−orbit-relativistic spin-restricted ZORA Hamiltonian as implemented in ADF 2000.01.[57] As a controle, spin-unrestricted quasi-relativistic computations of the g values were performed using the Pauli Hamiltonian, but otherwise the same basis sets as implemented in ADF 2002.01 was used.[58,59]

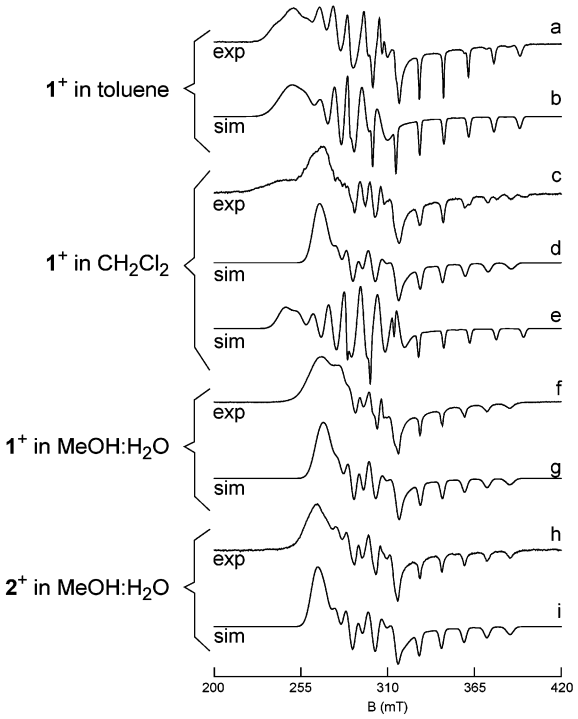

Figure 1. Experimental (a,c,f,h) and simulated (b,d,e,g,i) X-band CW-EPR spectra (9.43 GHz) taken at 120 K. (a) $\mathbf{1}^+$ in toluene. (b) Simulation of (a). (c) $\mathbf{1}^+$ in CH_2Cl_2. (d,e) Simulation of contributions *A* and *B* in (c) (see Table 1). (f) $\mathbf{1}^+$ in MeOH:H_2O. (g) Simulation of (f). (h) $\mathbf{2}^+$ in MeOH:H_2O. (i) Simulation of (h).

Results

Influence of the Solvent on the EPR Spectra of $\mathbf{1}^+$ and $\mathbf{2}^+$. Figure 1 shows the X-band CW-EPR spectra of $\mathbf{1}^+$ in toluene (1a), $\mathbf{1}^+$ in CH_2Cl_2 (1c), $\mathbf{1}^+$ in MeOH:H_2O (1f) and $\mathbf{2}^+$ in MeOH:H_2O (1h). It is clear that the change of the solvent has a strong influence on the spectra which is indicative of solvent ligation to the Co^{II} corrins. Furthermore, strong g and A strain effects are visible. The X-band spectra of $\mathbf{1}^+$ and $\mathbf{2}^+$ in MeOH:H_2O are very similar (compare Figure 1f with Figure 1h), which confirms the suitability of $\mathbf{1}^+$ as a model system for $\mathbf{2}^+$. Two components (*A* and *B*, Figure 1d,e) contribute to the CW-EPR spectrum of $\mathbf{1}^+$ in CH_2Cl_2 (Figure 1c), whereas the spectra of $\mathbf{1}^+$ in toluene and in MeOH:H_2O and $\mathbf{2}^+$ in MeOH:H_2O consist essentially of one species.

All X-band spectra could be satisfactorily simulated using axial **g** and $\mathbf{A}^{Co}$ matrixes and a large g and A strain (Table 1, Figure 1b,d,e,g,i). Nevertheless, as can be appreciated from Figure 1, the simulated spectra do not match exactly the experimental spectra. This might be due to a rhombicity of the **g** and cobalt hyperfine matrixes (which we would expect from

(44) Gromov, I.; Shane, J.; Forrer, J.; Rakhmatoullin, R.; Rozentzwaig, Yu.; Schweiger, A. *J. Magn. Reson*. **2001**, *149*, 196−203.
(45) Gromov, I.; Krymov, V.; Manikandan, P.; Arieli, D.; Goldfarb, D. *J. Magn. Reson*. **1999**, *139*, 8−17.
(46) Höfer, P.; Grupp, A.; Nebenführ, H.; Mehring, M. *Chem. Phys. Lett.* **1986,** *132*, 279−282.
(47) Szosenfogel, R.; Goldfarb, D. *Mol. Phys.* **1998**, *95*, 1295−1308.
(48) Madi, Z. L.; Van Doorslaer, S.; Schweiger, A. *J. Magn. Reson*. **2002**, *154*, 181−191.
(49) Davies, E. R. *Phys. Lett.* **1974**, *A47*, 1−2
(50) Mims, W. B. *Proc. R. Soc. London* **1965**, *283*, 452−457.
(51) Baerends, E. J.; Ellis, D. E.; Ros, P. *Chem. Phys*. **1973**, *2*, 41−51.
(52) Versluis, L.; Ziegler, T. *J. Chem. Phys*. **1988**, *88*, 322−328.
(53) te Velde, G.; Baerends, E. J. *J. Comput. Phys*. **1992**, *99*, 84−98.
(54) Fonseca Guerra, C.; Snijders, J. G.; te Velde, G.; Baerends, E. *Theor. Chem. Acc*. **1998**, *99*, 391−403.
(55) van Lenthe, E.; Snijders, J. G.; Baerends, E. J. *J. Chem. Phys*. **1996**, *105*, 6505−6516.
(56) Lide, D. R., Ed. *Handbook of Chemistry and Physics*, 76th ed.; CRC Press: Boca Raton, FL, 1995; Ch. 9, pp 84−86.
(57) van Lenthe, E.; Wormer, P. E. S.; van der Avoird, A. *J. Chem. Phys*. **1997**, *107*, 2488−2498.
(58) Schreckenbach, G.; Ziegler, T. *J. Phys. Chem. A* **1997**, *101*, 3388−3399.
(59) Patchkovskii, S.; Ziegler, T. *J. Chem. Phys*. **1999**, *111*, 5730−5740.

Table 1. g and A^{Cu} Principal Values of 1^+ and 2^+ in Different Solvents

	$g_\perp$ ($g_{x,y}$)	$g_\parallel$ (g_z)	$A_\perp$ [MHz] ($A_{x,y}$)	$A_\parallel$ [MHz] (A_z)	A strain[a] [MHz]	g strain[b]	ref
$\mathbf{1}^+$ in toluene	2.447	1.990	273	430	55/6	0.008/0.002	this work
$\mathbf{1}^+$ in CH_2Cl_2	2.327[c]	1.997[c]	210[c]	397[c]	30/20	0.0005/0	this work
	2.397[d]	1.986[d]	330[d]	445[d]	35/5	0.005/0.002	this work
$\mathbf{1}^+$ in methanol	2.327[e]	1.999[e]	217[e]	395[e]	30/20	0.0005/0	this work
	2.272[f]	2.004[f]	120[f]	380[f]	15/8	0.0005/0.0002	this work
$\mathbf{1}^+$ in MeOH:H_2O	2.320	1.997	200	390	35/20	0.002/0	this work
$\mathbf{2}^+$ in MeOH:H_2O	2.320	1.997	213	395	30/16	0.0006/0	this work
$Co^{II}(dmgH)_2$ in H_2O	2.31, 2.194	2.009	70, 20	328			61
B_{12r} (*base-on*)	2.31, 2.19	2.004	65, 80	302			30
CoTPP in toluene	2.930	1.925	780	420			35
	2.795	1.962	617	415			35
CoTPP in toluene/pyridine	2.324	2.030	<40	236			33

A comparison with Co(II) (tetraphenylporphyrin) (CoTPP) complexes in different matrices is given. [a] fwhh of the Gaussian distribution of $A_\perp$ and $A_\parallel$. [b] fwhh of the Gaussian distribution of $g_\perp$ and $g_\parallel$. [c] Component *A* (contributes 59% to the spectrum) [d] Component *B* (contributes 41% to the spectrum) [e] Component *C* [f] Component *D*, only observed below 100 K.

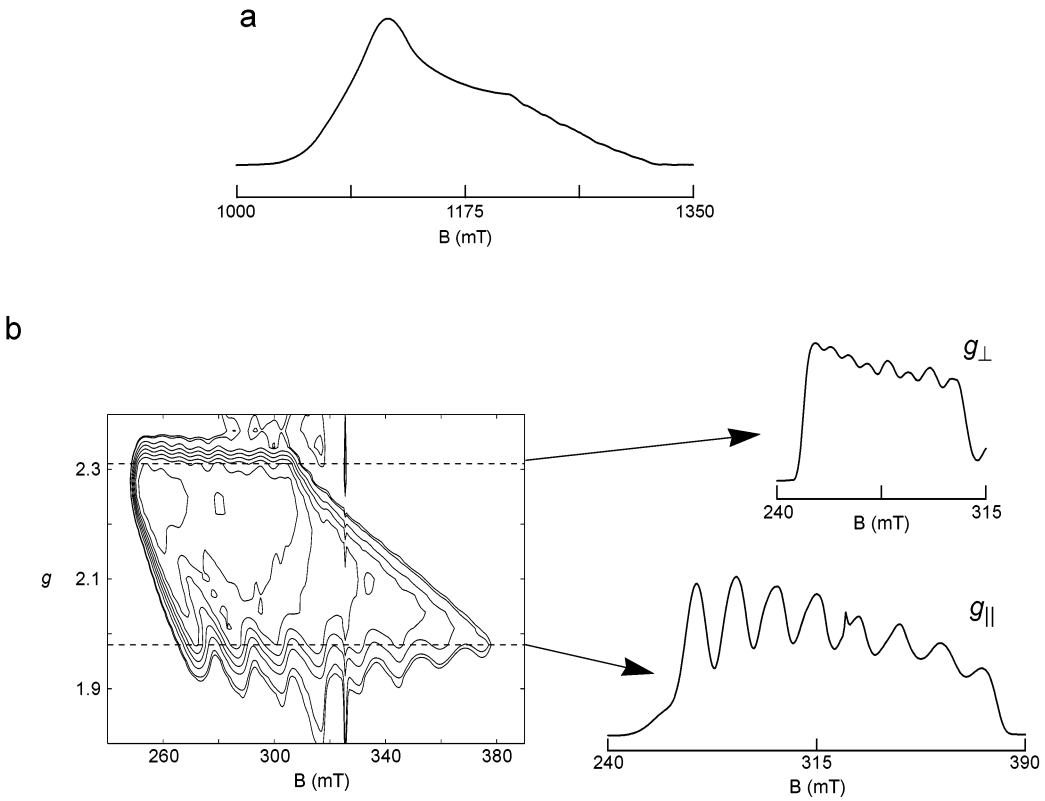

Figure 2. (a) Q-band ESE-detected EPR spectrum (35.28 GHz) of $\mathbf{1}^+$ in MeOH:H_2O taken at 15 K. (b) X-band EZ-EPR spectrum (9.15 GHz) of $\mathbf{2}^+$ in MeOH:H_2O at 15 K. Slices are shown at $g_\parallel$ and $g_\perp$.

symmetry considerations) and/or a complicated correlation of the g and A strain. To check the first possibility, echo-detected EPR spectra were taken at Q-band for all systems under study (e.g., Figure 2a, $\mathbf{1}^+$ in MeOH:H_2O), and all spectra corroborate axiality of **g** within the experimental error and confirmed again the large g-strain effects. For $\mathbf{2}^+$ in MeOH:H_2O, also an EZ-EPR spectrum was measured at X-band (Figure 2b) in order to take advantage of the enhanced orientation selectivity. Using the EZ-EPR method, the EPR spectrum can be spread into a second dimension, representing the g values. The form of the 2D spectrum shows again that, within the experimental error, the **g** and $\mathbf{A}^{Co}$ matrixes are axial. The EZ EPR spectrum allows for a better determination of $A_\perp$. Furthermore, it proves that both a large g strain (line width in the g-dimension) and a large A strain (visible in the slices at different g values) is present. It should be noted that neither with high-field EPR nor with EZ-EPR deviations from axiality smaller than the g- and A-strain effects can be detected.

In the spectrum of $\mathbf{1}^+$ in toluene (Figure 1a), only one component is observed (traces of a second component are found, which become stronger when the toluene is not dried extensively). The g and cobalt hyperfine values differ considerably from those of cobalt(II) (tetraphenyl)porphyrin (CoTPP) in toluene[35] (or in any other π-acceptor matrix) (Table 1). It is important to note that $|A_\parallel| > |A_\perp|$ for $\mathbf{1}^+$ in toluene but $|A_\parallel| < |A_\perp|$ for the 1:1 and 1:2 charge-transfer (CT) complexes of CoTPP in toluene. This observation suggests an axial ligation to a donor rather than to an acceptor ligand.[35,60] This is further corroborated by the fact that for $\mathbf{1}^+$ in toluene $g_\perp$ is substantially smaller than for the CoTPP:toluene CT-complexes. A possible

(60) Iwaizumi, M.; Ohba, Y.; Iida, I.; Hirayama, M. *Inorg. Chim. Acta* **1984**, *82*, 47−52.

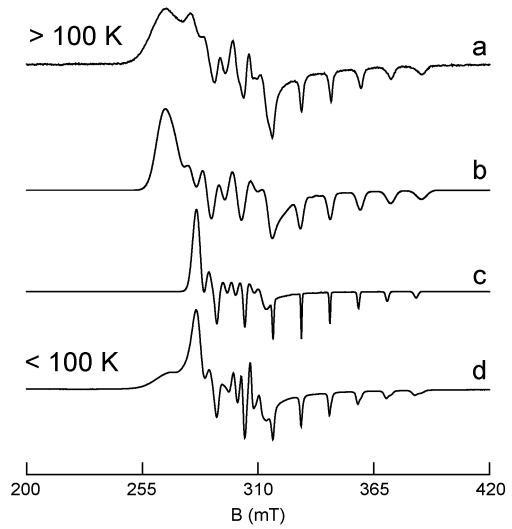

Figure 3. Experimental CW-EPR spectrum (9.43 GHz) of $\mathbf{1}^+$ in methanol at 120 K (a) and below 100 K (d). (b) Simulation of (a), contribution *C* in Table 1. (c) Simulation of contribution *D* (Table 1) present in low-temperature experimental spectrum (d).

explanation for this observation is that $\mathbf{1}^+$ forms a donor−acceptor pair with its counterion ClO_4^-.

Component *A* in the EPR spectrum of $\mathbf{1}^+$ in CH_2Cl_2 (Figure 1d) has EPR parameters close to those of $\mathbf{1}^+$ in MeOH:H_2O, whereas the EPR parameters of component *B* (Figure 1e) resemble those of $\mathbf{1}^+$ in toluene. This seems to indicate that CH_2Cl_2 was still not free of water, despite the drying procedure. The fact that the EPR parameters of component *B* are close to those of $\mathbf{1}^+$ in toluene supports the earlier assumption that $\mathbf{1}^+$ can form a contact-ion pair with perchlorate because CH_2Cl_2 is expected to be a poor ligand for a Co^{II} center.

The trend observed for the EPR parameters of $\mathbf{1}^+$ or $\mathbf{2}^+$ in MeOH:H_2O versus those of $\mathbf{1}^+$ in toluene agrees with an axial ligation of a σ-donor (methanol or water) to the Co^{II} center ($g_\perp$, $A_\perp$, and $A_{||}$ decrease, whereas $g_{||}$ increases). This is supported by the fact that this tendency continues when a strong Lewis base is coordinating to the cobalt(II) ion (see Table 1, DBI in *base-on* B_{12r}[30] and pyridine in CoTPPPy[33]). Bis(dimethylglyoximato) cobalt(II), $Co^{II}(dmgH)_2$, a frequently used model system for B_{12r}, has lower $g_{x,y}$, $A_{x,y}$, and A_z values and a higher g_z value as observed for $\mathbf{1}^+$ and $\mathbf{2}^+$ in MeOH:H_2O (Table 1[61]). It is known that $Co^{II}(dmgH)_2$ is ligated to two water molecules. This suggests that in the case of $\mathbf{1}^+$ and $\mathbf{2}^+$ in MeOH:H_2O only one solvent molecule is coordinating.

Solvent-Related Temperature-Dependent Effects for $\mathbf{1}^+$ in Methanol. Above 100 K, the X-band CW-EPR spectrum of $\mathbf{1}^+$ in methanol (Figure 3a) is similar to that of $\mathbf{1}^+$ in MeOH:H_2O (Figure 1f). Below 100 K the spectrum changes dramatically (Figure 3d). Although traces of the high-temperature component *C* (Table 1, Figure 3b) are still present, the spectrum is now dominated by a new component *D* (Table 1, Figure 3c). The temperature at which this transition occurs agrees with the phase-transition temperature of methanol for the transition of the crystalline α-phase to the glassy state (103 K).[62] The assumption that the EPR observation is related to the phase transition of the solvent was supported by changing the speed of the freezing. Sugisaki et al.[62] showed that by cooling methanol slowly to the glassy state, warming up again to a temperature slightly above 103 K, allowing for crystallization and subsequent quick cooling to 70 K or lower allows for the formation of a metastable crystalline phase at temperatures below the transition temperature. After application of this procedure to $\mathbf{1}^+$ in methanol, an EPR spectrum resembling largely the one shown in Figure 3a could be measured at temperatures lower than 100 K. Furthermore, the fact that this peculiar behavior is not observed for $\mathbf{1}^+$ in MeOH:H_2O supports the assumption that it is indeed the phase transition which causes the change in the EPR spectrum. Addition of water will change the phase-transition characteristics and, moreover, water makes a poor glass which explains the lack of component *D* in the spectra of $\mathbf{1}^+$ in MeOH:H_2O.

The *g* and cobalt hyperfine values of component *D* (Table 1, parameters determined from simulations) indicate that either a stronger ligation of the methanol molecule occurs than at higher temperature or that two methanol molecules are coordinating (compare with the data of $Co^{II}(dmgH)_2(H_2O)_2$ [61]). A reasonable assumption would be that the polar methyl ester substituents of $\mathbf{1}^+$ take part in the H-bond network formed in the crystalline α-phase of the methanol solvent. When the crystalline phase changes to the glassy state, this rigid network collapses and a new coordination situation may become feasible.

Influence of the Solvent on the Interactions with the Corrin Nitrogens. HYSCORE,[46] a two-dimensional pulse EPR experiment in which a mixing π pulse creates correlations between the nuclear coherences in two different electron spin (m_S) manifolds, is found to be the most appropriate method to study the magnetic parameters of the corrin nitrogens. The spin Hamiltonian of an $S = 1/2$, $I = 1$ system (e.g. ^{14}N) can be described in terms of the **g** matrix, the hyperfine matrix **A** and the nuclear quadrupole tensor **Q**. The principal values Q_x, Q_y and Q_z of the traceless **Q** tensor are usually expressed by the quadrupole coupling constant e^2qQ/h and the asymmetry parameter η with $Q_x = -(e^2qQ/4h)(1-\eta)$, $Q_y = -(e^2qQ/4h)(1+\eta)$ and $Q_z = e^2qQ/2h$. The HYSCORE spectra of disordered $S = 1/2$, $I = 1$ systems are dominated by the cross-peaks between the double-quantum (DQ) frequencies[63,64]

$$\nu_{\alpha,\beta}^{DQ} = 2((a/2 \pm \nu_I)^2 + (e^2qQ/4h)^2(3+\eta^2))^{1/2} \qquad (1)$$

where *a* is the hyperfine coupling at a particular observer position and ν_I is the nuclear Zeeman frequency.

X-band HYSCORE spectra were recorded at different observer positions for the systems under study. The spectra of $\mathbf{1}^+$ in toluene, in CH_2Cl_2 and in MeOH:H_2O and of $\mathbf{2}^+$ in MeOH:H_2O were found to be very similar. Figure 4a (4c) shows as a typical example the HYSCORE spectrum of $\mathbf{2}^+$ in MeOH:H_2O at observer position $g_\perp$ ($g_{||}$, $m_I = -7/2$). The cross-peaks between the double-quantum frequencies can clearly be identified in all spectra. Furthermore, cross-peaks involving single-quantum frequencies can be observed (e.g., Figure 4a, cross-peak at (4 MHz, 1 MHz) in (+,+) quadrant). The strong broadening of the cross-peaks, which is observed even at the

(61) Lubitz, W.; Winscom, C. J.; Diegruber, H.; Möseler, R. *Z. Naturforsch.* **1987**, *42a*, 970−986.
(62) Sugisaki, M.; Suga, H.; Syûzô, S. *Bull. Chem. Soc. Jpn.* **1968**, *41*, 2586−2591.
(63) Dikanov, S. A.; Xun, L.; Karpiel, A. B.; Tyryshkin, A. M.; Bowman, M. K. *J. Am. Chem. Soc.* **1996**, *118*, 8408−8416.
(64) Dikanov, S. A.; Tsvetkov, Yu. D.; Bowman, M. K.; Astashkin, A. V. *Chem. Phys. Lett.* **1982**, *90*, 149−153.

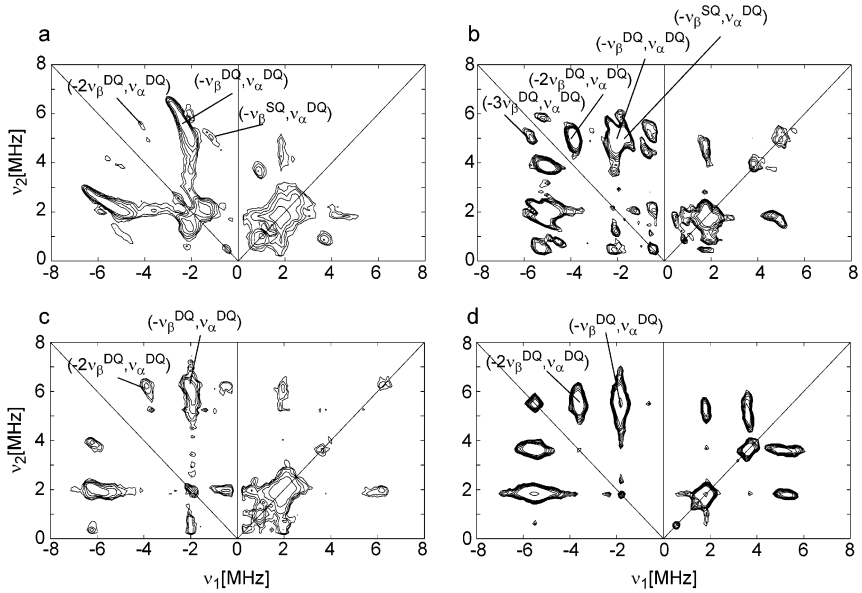

Figure 4. Experimental HYSCORE spectra of $\mathbf{2}^+$ in MeOH:H_2O (a, c) and of $\mathbf{1}^+$ in methanol (b,d) (9.71 GHz, $\tau = 96$ ns, see spectroscopy section). (a, b) Observer position corresponding to $g_\perp$ (c, d) Observer position corresponding to $g_{||}$, $m_I = -7/2$.

Table 2. ^{14}N Hyperfine and Nuclear Quadrupole Principal Values of the Pyrrole Nitrogens of 1^+ and 2^+ in Different Solvents[a]

	$\lvert A_{x'}\rvert$ [MHz] (± 0.3)	$\lvert A_{y'}\rvert$ [MHz] (± 0.3)	$\lvert A_{z'}\rvert$ [MHz] (± 0.3)	$\lvert e^2qQ/h\rvert$ [MHz] (± 0.1)	η (± 0.1)	ref
$\mathbf{1}^+$ in toluene	4.3	2.4	3.5	1.65	0.95	this work
$\mathbf{1}^+$ in CH_2Cl_2	4.2	2.3	3.5	1.65	0.95	this work
$\mathbf{1}^+$ in methanol	3.2	2.4	2.7	1.7	0.95	this work
$\mathbf{1}^+$ in MeOH:H_2O	4.4	2.2	3.5	1.7	0.95	this work
$\mathbf{2}^+$ in MeOH:H_2O	4.7	2.0	3.5	1.7	0.95	this work
CoTPP in toluene	3.7	3.7	4.3	1.8	0.50	35
CoTPP in toluene/pyridine	4.07	2.43	2.85	1.8	0.55	33
$Co^{II}(dmgH)_2$ in methanol	2.53	1.9	1.9	3.4	0.7	80

[a] x' and y' lie in the molecular plane, z' is parallel to $g_{||}$. The largest nuclear quadrupole value lies along x', the smallest along z'.

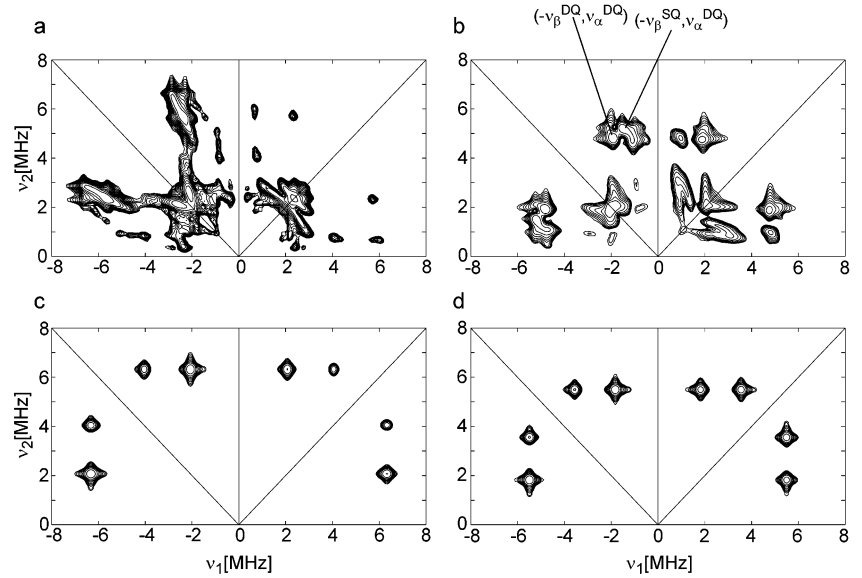

Figure 5. Simulations corresponding to the experimental HYSCORE spectra in Figure 4. Simulation parameters are given in Table 2.

high-field single-crystal position (Figure 4c), suggests a distribution of the hyperfine values (small inequivalence of the 4 corrin nitrogens) and/or a considerable A- and Q-strain effect (see the Supporting Information, Figure S1). In the (-,+) quadrant of the HYSCORE spectra cross-peaks of the type $(-2\nu_\beta^{DQ}, \nu_\alpha^{DQ})$ occur confirming that the observed signals arise from at least 2 quasi-equivalent nuclei. In Table 2 the hyperfine and nuclear quadrupole interactions of the corrin nitrogens of $\mathbf{1}^+$ in toluene, in CH_2Cl_2 and in MeOH:H_2O and of $\mathbf{2}^+$ in MeOH:H_2O are given. Figure 5a,c show the simulations of the spectra in Figure 4a,c, whereby the full parameter set of Table 2 was used including the tensor principal directions. All simulations were done assuming ideal pulses, which explains the differences in relative peak intensities between experiment and simulation. To

reduce the computation time, the simulations were performed for only one nitrogen nucleus (Figure 5a, observer position $g_\perp$ to which a large amount of orientations contribute) or two nitrogens (Figure 5c, observer position with highest orientation selectivity). In the latter case, the **A** and **Q** tensor of the second nitrogen were turned 90° in the corrin plane to simulate the contribution of two adjacent nitrogens of the corrin ring.

Figure 4, parts b and d, depict the HYSCORE spectra of $\mathbf{1}^+$ in methanol at the observer positions $g_\perp$ and $g_{||}$, $m_I = -7/2$. The HYSCORE spectra have changed dramatically (compare to Figure 4a,c). The in-plane anisotropy of the hyperfine coupling is reduced significantly (compare ridge form of the ($-\nu_\beta^{DQ}$, ν_α^{DQ}) peaks in Figure 4, parts a and c). The cross-peaks ($-2\nu_\beta^{DQ}$, ν_α^{DQ}) and ($-3\nu_\beta^{DQ}$, ν_α^{DQ}) in the (−,+) quadrant show that at least three quasi-equivalent nitrogen nuclei contribute to the spectrum, confirming again the assignment of these signals to the corrin nitrogens. Such ($-3\nu_\beta^{DQ}$, ν_α^{DQ}) cross-peaks are rarely detected in disordered systems without using special matched pulses in the HYSCORE sequence.[65] The ^{14}N hyperfine and nuclear quadrupole parameters of $\mathbf{1}^+$ in methanol are given in Table 2. Again, the same restrictions on the simulation conditions were taken into account as mentioned before (Figure 5b,d).

The clear difference in the HYSCORE spectra of $\mathbf{1}^+$ in methanol compared to those of the other systems under study, indicates that fundamental changes must have taken place in the coordination of the Co^{II} ion. The change in the axial ligation and/or structure must be so dramatic that it even reflects in the magnetic parameters of the corrin nitrogens. This is surprising because the variation of the solvent from a MeOH:H_2O mixture to the apolar toluene had only minor influence on the couplings of the corrin nitrogens.

Finally, it should be noted that the sign of the hyperfine interactions cannot be derived from the HYSCORE spectra. For reasons mentioned later, we have taken the hyperfine values to be negative, in which case the smaller DQ frequency is the one in the β ($m_S = -1/2$) manifold.

Direct Proof of Solvent Interaction. In general, weak proton hyperfine interactions can best be determined using ENDOR techniques. To prove the axial ligation of solvent molecules for $\mathbf{1}^+$ and $\mathbf{2}^+$ in polar solvents, different ENDOR experiments were undertaken at X- and W-band mw frequencies. Figure 6 shows a comparison between the W-band Davies-ENDOR ^{1}H-spectra of $\mathbf{1}^+$ in CH_3OH (6a), $\mathbf{1}^+$ in CD_3OD (6b) and $\mathbf{1}^+$ in toluene (6c) at observer position $g = 1.99$ ($\sim g_{||}$). The proton-ENDOR spectrum of $\mathbf{1}^+$ in methanol clearly changes upon deuteration of the solvent. There is a large reduction of the central ENDOR signal at the nuclear Zeeman frequency, ν_H, which corresponds to a reduction of the number of protons at larger distance. Furthermore, ENDOR signals corresponding to hyperfine couplings of 3−6 MHz disappear (see dashed line, Figure 6), which proves that these signals arise from solvent protons interacting significantly with the unpaired electron. These interactions are specific for the polar solvent as can be seen from comparison with Figure 6c. The ENDOR spectra of $\mathbf{1}^+$ in toluene resemble closely those of $\mathbf{1}^+$ in CD_3OD (compare Figure 6c with 6b). Their main difference lies in the fact that now a clear ENDOR signal is observed at ν_H, stemming from distant

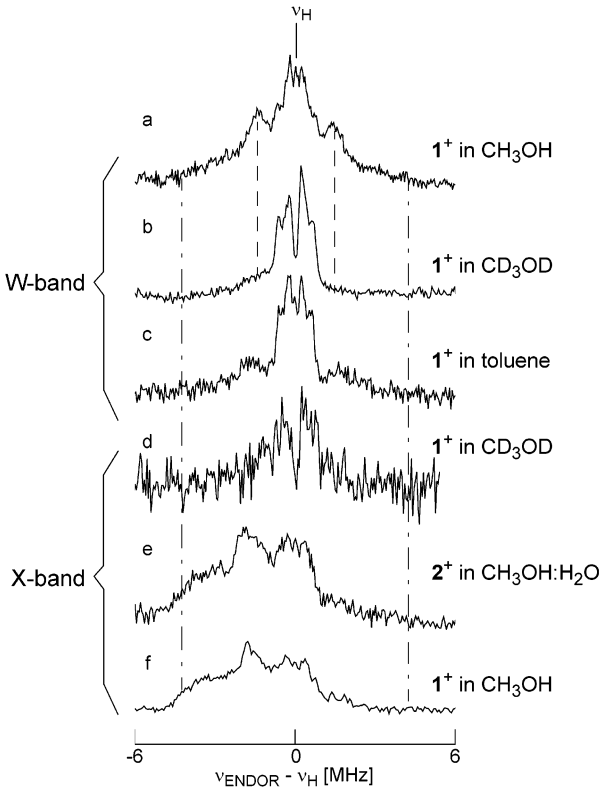

Figure 6. ^{1}H Davies-ENDOR spectra taken at an observer position corresponding to $g_{||}$, $m_I = -7/2$. Mw pulse lengths of $t_{\pi/2} = 50$ (100) ns, $t_\pi = 100$ (200) ns, and time intervals $\tau = 350$ (400) ns and $T = 13.5$ (20) μs were used at X (W) band. (a) $\mathbf{1}^+$ in CH_3OH, W-band ENDOR. (b) $\mathbf{1}^+$ in CD_3OD, W-band ENDOR (20 scans). (c) $\mathbf{1}^+$ in toluene, W-band ENDOR. (d) $\mathbf{1}^+$ in CD_3OD, X-band ENDOR (2000 scans). (e) $\mathbf{2}^+$ in CH_3OH:H_2O, X-band ENDOR. (f) $\mathbf{1}^+$ in CH_3OH, X-band ENDOR.

solvent protons. The weak signal (3 MHz) coupling which is still visible in the ENDOR spectrum of $\mathbf{1}^+$ in toluene (Figure 6c) is due to traces of H_2O in toluene (also visible in the corresponding EPR spectra).

The comparison of the Davies-ENDOR spectra of $\mathbf{1}^+$ in CD_3-OD taken at X-band (Figure 6d) and at W-band (Figure 6b) shows one of the advantages of high-field ENDOR. Although the experimental conditions were optimized in both cases, the ENDOR sensitivity and the spectral resolution are clearly superior at W-band.

Figures 6e and 6f show the X-band ENDOR spectrum of $\mathbf{2}^+$ in MeOH:H_2O and $\mathbf{1}^+$ in methanol at an observer position near $g_{||}$, $m_I = -7/2$. Although at this observer position, both the W-band and X-band ENDOR spectra of $\mathbf{1}^+$ in MeOH and $\mathbf{1}^+$ and $\mathbf{2}^+$ in MeOH:H_2O showed asymmetric line intensities, the asymmetry is largest at X-band (the ENDOR intensity became almost zero for frequencies larger than ν_H, see Figure 6e,f). The asymmetry of the W-band ENDOR spectra could clearly be attributed to a saturation of the nuclear transitions, because lengthening of the repetition time led to more symmetric spectra.[66] Furthermore, this asymmetry can also be used to obtain an indication of the absolute sign of the hyperfine interaction.[66] At observer position $g_{||}$ the 3−6 MHz couplings were found to be positive. At X-band, the spectral asymmetry is unlikely to be due to the saturation of the nuclear transitions

(65) Jeschke, G.; Rakhmatullin, R.; Schweiger, A. *J. Magn. Reson.* **1998**, *131*, 261−271.

(66) Epel, B.; Pöppl, A.; Manikandan, P.; Vega, S.; Goldfarb, D. *J. Magn. Reson.* **2001**, *148*, 388−397.

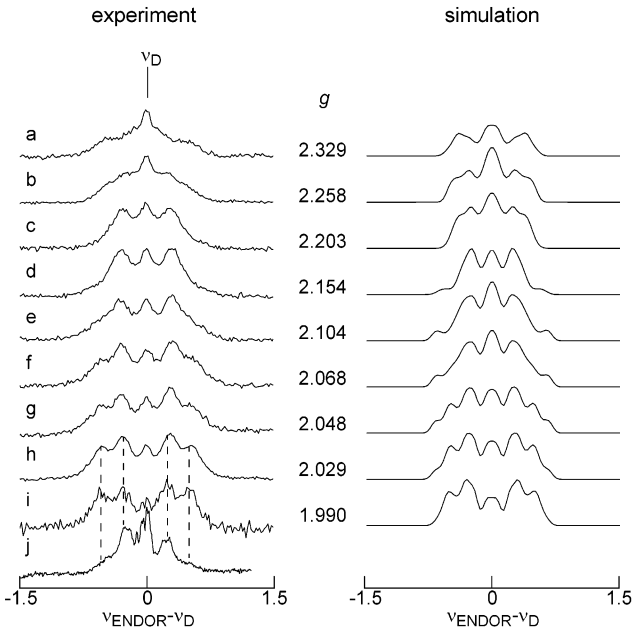

Figure 7. (a−i) W-band ^{2}H Mims-ENDOR spectra of $\mathbf{1}^+$ in CD_3OD at different observer positions (τ = 200 ns, other settings: see spectroscopy part). Left: experiment. Right: simulation. (j) The difference spectrum between the ^{1}H Davies-ENDOR spectra of $\mathbf{1}^+$ in CH_3OH and CD_3OD (frequency axis scaled by $g_{n,D}/g_{n,H}$) at an observer position corresponding to g = 2.029.

because this effect depends mainly on thermal polarization, which is low at X-band and 15 K. Possibly, baseline-related problems due to the low signal intensity lie at the bottom of the observed asymmetry.

Contrary to the expectations, the Davies-ENDOR spectra of $\mathbf{1}^+$ and $\mathbf{2}^+$ in MeOH:H_2O did not differ significantly from those of $\mathbf{1}^+$ in methanol (compare Figure 6e with 6f). The similarity is surprising and seems to contradict the assumption that the change in g and cobalt hyperfine values of $\mathbf{1}^+$ in MeOH at temperatures below 100 K arises from a stronger axial solvent coordination with consequent larger ^{1}H hyperfine interaction.

Further evidence for an interaction with the solvent molecule in $\mathbf{1}^+$ in CD_3OD is obtained from Mims-ENDOR ^{2}H-spectra taken at W-band (Figure 7a-i). ^{2}H interactions can also be determined using X-band HYSCORE spectroscopy (Figure S2, Supporting Information). HYSCORE can give additional information on the relative sign of the hyperfine values through the observed combination frequencies. Analysis of the HYSCORE spectra showed that at observer position $g_{||}$, $m_I = -7/2$, the corrin nitrogen and methanol deuterium hyperfine interactions have opposite sign (see the Supporting Information).

To simulate the ENDOR spectra in Figure 7, the number of ^{2}H nuclei contributing to the spectrum have to be determined. From the comparison with the X-band HYSCORE spectra (Figure S2, S3, S4), we already found that the central signal at the nuclear Zeeman frequency, ν_D, is mainly due to the methyl deuterium nuclei. The remaining four-line pattern observed in Figure 7i, might be due to the interaction of one nucleus with resolved nuclear quadrupole splitting (option 1) or of two nuclei with unresolved nuclear quadrupole interactions (option 2). Figure 7j shows the difference proton-ENDOR spectrum of $\mathbf{1}^+$ in CH_3OH and $\mathbf{1}^+$ in CD_3OD, whereby the frequency axis is scaled by $g_{n,D}/g_{n,H}$ (observer position g = 2.029). If option 2 is valid this spectrum should again give the four-line pattern, whereas for option 1 only two lines would remain. Clearly, we observe the interaction with two different types of ^{2}H nuclei (option 2). In Figure 7 (right) the simulations of the experimental spectra are shown using the parameters given in Table 3. For these simulations, the interactions with three types of nuclei were considered (two acidic deuterium nuclei and one methyl deuterium). The hyperfine couplings were checked by a simultaneous simulation of the difference-ENDOR spectra of $\mathbf{1}^+$ in CH_3OH and CD_3OD. These difference spectra contain only the ENDOR lines of the solvent protons. The maximum hyperfine values for the methyl deuterium (and corresponding proton) nuclei were estimated from the difference HYSCORE spectra of $\mathbf{1}^+$ in CD_3OH (see Figure S4C). For all deuterium nuclei initial guesses for the nuclear quadrupole values were taken from the nqr data of methanol.[67,68] A central line was added to mimic the contribution of the distant matrix protons. It is important to mention here that two types of acidic protons were also found for $\mathbf{1}^+$ and $\mathbf{2}^+$ in MeOH:H_2O (see e.g., Figure 6e) and that for both solvents the hyperfine interactions are the same within the experimental error. The EPR parameters of the acidic proton $H^{(1)}$ are close to those found for equatorially bound water in the $[Cu(H_2O)_6]^{2+}$ complex.[69]

To investigate whether ClO_4^- ligation is taking place in $\mathbf{1}^+$ in toluene, both Davies- and Mims-ENDOR experiments were carried out at X-band and W-band to find evidence of an interaction with the ^{35}Cl/^{37}Cl nuclei of ClO_4^-. No traces of such an interaction were found. Also, the HYSCORE spectra showed no sign of such an interaction. This does not exclude, however, the assumption of the contact-ion pair. If no strong bond is formed between cobalt and oxygen, but the interaction between cobester and perchlorate is more electrostatic, only little spin density is expected on the Cl nucleus. This will be further discussed on basis of DFT results (see below). Furthermore, it cannot be ruled out that unfavorable relaxation mechanisms prevented detection of the Cl-ENDOR or ESEEM.

Interactions with Protons of the Corrin Ligand. From the ENDOR spectra of $\mathbf{1}^+$ in CD_3OD the proton hyperfine couplings of the corrinoid ligand can in principle be determined (Figure 8a−f). Most of the observed ENDOR signals show splittings of less than 2 MHz. Due to the large amount of protons in the cobester ligand, it is not possible to identify each of them. One proton coupling, however, catches the eye (marked with the dashed lines in Figure 8). It varies from a maximal splitting of about 7 MHz for the in-plane observer positions to about 2.5 MHz at an observer position near the axial bond. This suggests that the interaction stems from a proton that is quasi in the corrin plane. Comparison with the ENDOR spectra of $\mathbf{1}^+$ in other solvents (e.g., Figure 6c, $\mathbf{1}^+$ in toluene) confirmed that the discussed interaction is due to a proton in the macrocycle and does not vary much upon change of the solvent.

Figure 8 (right) shows the simulations of this contribution using $A_{x'}$ = 7.0 (± 0.5) MHz, $A_{y'}$ = 3.0 MHz ($|A_{y'}| < 5.0$ MHz), $A_{z'}$ = 2.8 (± 0.5) MHz and $\beta = 10°$ (± 10°). β is the angle between $\boldsymbol{A}_{z'}$ and the plane normal for a rotation around $\boldsymbol{y}'$. It should be noted that the error for $A_{y'}$ is much larger because this signal is overlapping with the spectra of the other corrin protons (Figure 8a). Considering the structure of $\mathbf{1}^+$ (Scheme

(67) Clymer, J. W.; Ragle, J. L. *J. Chem. Phys.* **1982**, *77*, 4366−4373.
(68) Brett, C. R.; Edmonds, D. T. *J. Magn. Reson.* **1982**, *49*, 304−311.
(69) Atherton, N. M.; Horsewill, A. *J. Mol. Phys.* **1979**, *37*, 1349−1361.

Table 3. Experimental Hyperfine and Nuclear Quadrupole Principal Values of the Protons of the Ligating Methanol Molecules in 1^+ in Methanol[a]

	$A_{x'}$ [MHz] (±0.5)	$A_{y'}$ [MHz] (±0.5)	$A_{z'}$ [MHz] (±0.5)	β_1 (deg) (±10)	$Q_{x''}$ [kHz] (±10)	$Q_{y''}$ [kHz] (±10)	$Q_{z''}$ [kHz] (±10)	β_2 (deg) (±10)
acidic $H^{(1)}$	∓7.0	∓4.0	±8.0	20	−50	−80	130	60
acidic $H^{(2)}$	±3.0	±5.0	±3.4	25	−40	−90	130	80
methyl H	0.3	0.3	0.3	25	−40	−40	80	80

[a] Hyperfine values are given for ^{1}H nuclei, nuclear quadrupole values for the corresponding ^{2}H nuclei. β_1 (β_2) defines the angle between the $A_{z'}$ ($Q_{z'}$) axis and the $g_{||}$ axis.

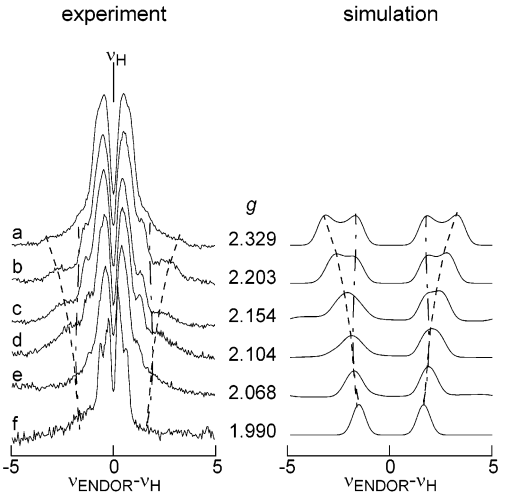

Figure 8. W-band ^{1}H Davies-ENDOR spectra of $\mathbf{1}^+$ in CD_3OD at different observer positions. Mw pulse lengths of $t_{\pi/2} = 100$ ns, $t_\pi = 200$ ns, and time intervals $\tau = 400$ ns and $T = 20$ μs were used. Experimental (left) and simulated spectra (right).

1), different (quasi-) in-plane protons can cause this interaction. The most obvious ones are the C_α proton (H19) or the H10-meso proton, but also the C_β protons (H3, H8, H13, H18) have to be considered (the atoms are numbered as in Scheme 1, based on the recommendations by the joint commission on biochemical nomenclature of IUPAC and IUB, section on the nomenclature of tetrapyrroles[70]).

Supporting Density Functional Computations. To elucidate some of the experimental observations, DFT computations of Co^{II} corrin ($\mathbf{3}^+$) with different axial ligands were undertaken ($\mathbf{3}^+ClO_4^-$, $\mathbf{3}^+(H_2O)$, $\mathbf{3}^+(MeOH)$, $\mathbf{3}^+(H_2O)_2$, $\mathbf{3}^+(MeOH)_2$). For the pentacoordinated complexes, the axial ligand was taken to coordinate from the less-hindered β-face. For all complexes, the correct d_z2 ground state was predicted. Although for the cobalt hyperfine values of all complexes under study $|A_z| > |A_{x,y}|$, the computed values deviated largely from the experimental ones (compare Table 1 with Table S1, Supporting Information). It has been reported earlier that the DFT computation of metal hyperfine values can be problematic, despite the reasonable results (±15%) found for less critical cases.[71] Furthermore, the hyperfine matrix is found to be orthorhombic, but the deviation from orthorhombicity falls within the experimental error (note the large *A* strain in the experimental spectra, Table 1). Interestingly, the cobalt hyperfine values are smaller for $\mathbf{3}^+ClO_4^-$ than for the other computed complexes, whereas we found larger hyperfine values for $\mathbf{1}^+$ in toluene than in polar solvents. From chemical intuition we would expect that in toluene a contact-ion pair is formed. The computations are not sufficiently accurate to rule this out because neither solvent effects nor the ring substituents were taken into account. It is to be expected that the influence of the polar methyl ester substituents is not negligible.

From the comparison of Table 1 and Table S1, it becomes clear that also the *g* values computed using the ZORA Hamiltonian[57] are not correctly predicted, although the trends $g_z < g_{x,y}$ and $g_z < g_e$ agree with the experiments of the different complexes. Again a significant orthorhombicity of the **g** matrix was found (larger than the experimental *g*-strain effect). Analogous remarks about the trend in *g* values for $\mathbf{3}^+ClO_4^-$ compared to the other computed complexes can be made as for the cobalt hyperfine values. When the Schreckenbach and Ziegler approach[58] was used to compute the *g* values, the agreement with the experiment became even worse (Table S1). The **g** anisotropy was underestimated by about a factor of 2 and $g_z > g_e$ was found in contradiction to the experiments.

It is clear from Table S1 that substitution of a water molecule by a methanol molecule has little effect on the *g* and cobalt hyperfine values. This agrees with the similarity in EPR parameters between $\mathbf{1}^+$ in MeOH:H_2O and in methanol (above 100 K). The EPR parameters of the five- and six-coordinated complexes are, however, clearly different ($g_{x,y}$ and $A_{x,y}$ are reduced, whereas g_z and A_z are increased). With the exception of the observation for A_z this corresponds to the trend observed in $\mathbf{1}^+$ in methanol above and below 100 K (component *C* versus *D*, Table 1).

Despite the poor agreement between the experimental and the computed *g* and metal hyperfine values, recent studies have shown that DFT can be used successfully in the computation of the *ligand* hyperfine and nuclear quadrupole values.[72,73] In Table 4, the computed hyperfine and nuclear quadrupole interactions of the corrin nitrogens are given for $\mathbf{3}^+ClO_4^-$, $\mathbf{3}^+(MeOH)$, $\mathbf{3}^+(MeOH)_2$, $\mathbf{3}^+(H_2O)$, and $\mathbf{3}^+(H_2O)_2$ are reported. The absolute values of the hyperfine couplings fall in the range observed experimentally. All hyperfine values are negative. This is valuable information since the HYSCORE technique does not allow for a determination of the absolute sign of the hyperfine interactions. The hyperfine interactions of the four nuclei are found to be inequivalent. Due to the large *A*-strain effect and the corresponding broad lines in the HYSCORE spectra (see Figure 4), such an inequivalence cannot be resolved experimentally. Furthermore, it is found that $A_{z'}$ is tilted away from the complex normal. This was not observed experimentally, but it should be noted that such a tilt is possible (the earlier mentioned strain effects reduce the attainable experimental accuracy).

For two of the corrin nitrogens (nitrogens of the A and D ring), e^2qQ/h is found to be positive with the largest principal value in-plane perpendicular to the $Co-N_{corrin}$ bond; for the

(70) Kräutler, B. In ref 3, pp 517−522.
(71) Munzarová, M.; Kaupp, M. *J. Phys. Chem. A* **1999**, *103*, 9966−9983.
(72) Neese, F. *J. Phys. Chem. A* **2001**, *105*, 4390−4299.
(73) Harmer, J.; Van Doorslaer, S.; Gromov, I.; Bröring, M.; Jeschke, J.; Schweiger, A. *J. Phys. Chem. B* **2002**, *106*, 2801−2811.

Table 4. Computed Hyperfine and Nuclear Quadrupole Principal Values of the Corrin Nitrogens for Different Co^{II} Corrin Complexes (BLYP/ZORA V)[a]

	$A_{x'}$ [MHz]	$A_{y'}$ [MHz]	$A_{z'}$ [MHz]	β_3 (deg)	$Q_{x''}$ [MHz]	$Q_{y''}$ [MHz]	$Q_{z''}$ [MHz]
$\mathbf{3}^+ClO_4^-$	−4.14	−3.61	−1.95	69.3	−0.85	−0.02	0.87
	−2.66	−2.08	−0.56	52.9	−1.01	0.18	0.83
	−3.47	−3.13	−1.27	59.5	−0.97	0.15	0.82
	−4.21	−3.60	−2.58	68.8	−0.80	−0.08	0.88
$\mathbf{3}^+$(MeOH)	−4.48	−3.95	−2.50	72.4	−0.77	−0.13	0.89
	−3.58	−2.97	−2.17	57.5	−0.95	0.15	0.80
	−3.75	−3.42	−1.97	55.8	−0.90	0.08	0.82
	−4.40	−3.79	−2.82	68.2	−0.76	−0.10	0.86
$\mathbf{3}^+(MeOH)_2$	−2.60	−2.81	−3.61	75.8	−0.79	−0.11	0.91
	−2.97	−2.53	−1.98	10.0	0.83	0.14	−0.97
	−3.21	−2.75	−2.20	13.4	0.84	0.10	−0.94
	−2.95	−3.08	−3.90	72.8	−0.79	−0.08	0.87
$\mathbf{3}^+(H_2O)$	−4.44	−3.90	−2.42	71.8	−0.77	−0.11	0.89
	−3.61	−3.02	−2.22	55.9	−0.95	0.14	0.81
	−3.68	−3.36	−1.87	55.0	−0.89	0.07	0.83
	−4.29	−3.67	−2.68	65.8	−0.76	−0.09	0.86
$\mathbf{3}^+(H_2O)_2$	−2.53	−2.58	−3.46	76.2	−0.79	−0.11	0.90
	−3.11	−2.67	−2.11	11.2	−0.96	0.14	0.82
	−3.09	−2.65	−2.06	15.9	−0.93	0.06	0.87
	−2.74	−3.05	−3.80	73	−0.79	−0.14	0.92

[a] z' makes an angle β_3 with the $Co-N_{Corrin}$ bond. x' is in the macrocycle plane, approximately perpendicular to the $Co-N_{Corrin}$ bond. x'' (z'') lies in the corrin plane parallel (perpendicular) to the $Co-N_{Corrin}$ bond.

other two corrin nitrogens, e^2qQ/h is negative and the negative principal value lies along the $Co-N_{corrin}$ bond. Although the changes seem drastic, they are actually caused by small changes of $Q_{y''}$ from a small negative to a small positive value which in turn leads to a change in the sign of e^2qQ/h per definition. Relative small local changes in the electric field gradient principal component perpendicular to the macrocycle can cause $Q_{y''}$ to change. As shown by Brown and Hoffman,[74] the largest nuclear quadrupole principal value lies along the metal-N bond when e^2qQ/h is negative, whereas it is perpendicular to this bond in the plane when e^2qQ/h is positive. This explains nicely the observed behavior. Experimentally, it is found that the axis of the nitrogen nuclear quadrupole tensor that corresponds to the largest principal value lies in the plane and that η is close to 1 (thus also small $|Q_{y''}|$) (Table 2). In the Supporting Information, the SOMO, the spin density distribution and the structure of $\mathbf{3}^+$(MeOH) are shown and discussed (Figure S5). There seems to be a correlation between the nuclear quadrupole interactions for the four nitrogens and the ring distortions.

Upon ligation of a second solvent molecule (water or methanol), the nuclear quadrupole values are found to remain unaffected, whereas the anisotropy of the hyperfine matrix is reduced. This is similar to the observation for $\mathbf{1}^+$ in methanol (Table 2).

Table 5 gives a list of the computed proton hyperfine couplings for H10 (meso-proton), H19 (C_α proton) and H3 (a typical example of a C_β proton). It is clear that only H19 agrees with the experimental couplings found for one of the corrin ligand protons (dashed lines in Figure 8). Furthermore, these couplings do not vary drastically upon change of the β ligand, in agreement with the experiment. Addition of a second α ligand reduces the spin density at the H19 proton, but the general anisotropy of the hyperfine matrix still agrees with the one observed experimentally.

(74) Brown, T. G.; Hoffman, B. M. *Mol. Phys.* **1980**, *39*, 1073−1109.

Table 5. Computed Proton Hyperfine Principal Values of Ring Protons for Different Co^{II} Corrin Complexes (BLYP/ZORA V)[a]

	nucleus	$A_{x'}$ [MHz]	$A_{y'}$ [MHz]	$A_{z'}$ [MHz]
$\mathbf{3}^+ClO_4^-$	H10	−2.33	−1.38	1.23
	H19	−0.24	0.19	6.33
	H3	−0.95	−0.92	0.72
$\mathbf{3}^+(H_2O)$	H10	−1.89	−1.21	1.45
	H19	−0.10	0.20	6.33
	H3	−1.45	−1.40	0.29
$\mathbf{3}^+$(MeOH)	H10	−1.92	−1.21	1.44
	H19	−0.13	0.20	6.30
	H3	−1.46	−1.41	0.27
$\mathbf{3}^+(H_2O)_2$	H10	−1.31	−0.85	1.62
	H19	−1.29	−1.06	5.13
	H3	−1.76	−1.71	−0.04
$\mathbf{3}^+(MeOH)_2$	H10	−1.34	−0.87	1.60
	H19	−1.31	−1.03	5.24
	H3	−1.77	−1.71	−0.04

[a] $A_{z'}$ is approximately along the H−Co direction. For the numbering of the ring, see ref 70 and Scheme 1.

In Table S2, the computed hyperfine (and nuclear quadrupole) values of the solvent protons (^2H nuclei) are given. Comparison with Table 3 tells us that the hyperfine data of the experimentally observed acidic $H^{(1)}$ of $\mathbf{1}^+$ in methanol agree well with those computed for the acidic proton in $\mathbf{3}^+$(MeOH). The assignment of the signs of the hyperfine values is now also evident. Our HYSCORE analysis revealed that at the observer position near the normal of the plane, the corrin nitrogen and the proton (deuterium) hyperfine values have opposite signs. From the asymmetric behavior of the W-band ENDOR signals, a positive hyperfine value was derived for the protons at this observer position. Indeed, in the computation $A_{z'}^H$ is near the complex normal and has a positive value, whereas the nitrogen hyperfine interaction is negative.

Furthermore, the hyperfine couplings of the acidic solvent molecules are slightly reduced upon addition of a second ligand at the α-face, but, considering the large *g*- and *A*-strain effects observed experimentally, it is fair to say that addition of a second solvent ligand may induce only little changes in the proton ENDOR spectra.

There is a clear difference between the experimentally observed hyperfine couplings for the methyl protons of methanol and those computed with DFT. Even if we assume that the computed individual differences between the three protons will be averaged out in the experiment, then the obtained values are still higher than those observed. The neglect of interactions of the primary complex with further solvent molecules might be responsible for this disagreement as such interactions are expected to be fairly strong in a hydrogen-bonding solvent.

The second acidic $H^{(2)}$ (Table 3), which was present for $\mathbf{1}^+$ in $MeOH:H_2O$ and in methanol and for **2** in $MeOH:H_2O$ could not be identified from the computations. The hyperfine anisotropy of this proton is well below the one of $H^{(1)}$ and of the computed hyperfine matrixes. It should be stressed again that for the DFT computations, the ring substituents were not taken into account. An NMR analysis of aquocobalamin showed that a hydrogen bond was formed between the cobalt coordinated water molecule and the carbonyl oxygen of the c-acetamide side chain. Such a hydrogen bond will significantly influence the EPR parameters of the acidic proton.[75]

(75) Kratky, C.; Färber, G.; Gruber, K.; Wilson, K.; Dauer, Z.; Nolting, H.-F.; Konrat, R.; Kräutler, B. *J. Am. Chem. Soc.* **1995**, *117*, 4654−4670.

For $\mathbf{3}^{+}ClO_4^{-}$, the ^{35}Cl hyperfine interaction was found to be [5.29, 5.55, 8.20] MHz, with a nuclear quadrupole interaction $e^2qQ/h = 1.37$ MHz and $\eta = 0.787$. Experimentally, no interaction with the Cl nucleus could be observed. This supports the earlier assumption that no strong bond between Co and an oxygen of perchlorate is formed, but does not rule out weak contact-ion pair formation.

Discussion

The major outcome of the present studies is that the EPR parameters of *base-off* Co^{II} corrins show a clear solvent dependence, establishing the often presumed presence of axial (solvent) ligation.[76] This finding is important because *base-off* cobalt(II) corrinates are often addressed as being four-coordinated.[4,22]

The *g* and cobalt hyperfine values of $\mathbf{1}^{+}$ in toluene are typical for an axial ligation of a weak donor rather than an acceptor ligand, in agreement with the expected tendency of $\mathbf{1}^{+}$ to form a contact-ion pair with ClO_4^{-} in apolar solvents. This is confirmed by the fact that in the EPR spectrum of $\mathbf{1}^{+}$ in CH_2Cl_2 a component (*A*) with similar characteristics is found. Because the nature of the solvent will influence the strength of the contact-ion pair it is not surprising that the EPR parameters for $\mathbf{1}^{+}$ in toluene and CH_2Cl_2 differ. Furthermore, the X-ray crystal structure of $\mathbf{1}^{+}ClO_4^{-}$ showed axial coordination of perchlorate to the cobalt(II) ion (Co−O distance 0.231 nm).[6] DFT computations for $\mathbf{3}^{+}ClO_4^{-}$ predict a considerable hyperfine interaction with the Cl nucleus, which is not observed experimentally. However, the geometry optimization for $\mathbf{3}^{+}ClO_4^{-}$ gives a Co−O distance of 0.222 nm which is less than the one observed in the single crystals of $\mathbf{1}^{+}ClO_4^{-}$.[6] Considering that the solvent will even further influence the length of the axial bond, it is very likely that the DFT computation underestimates the Co−O distance and thus overestimates the expected hyperfine coupling to the chlorine. Furthermore, the hyperfine and nuclear quadrupole interactions are expected to be broadly distributed for a contact-ion pair in a glassy matrix and the corresponding signals may therefore have escaped detection.

The *g* and cobalt hyperfine values of $\mathbf{1}^{+}$ in methanol, MeOH:H_2O and $\mathbf{2}^{+}$ in MeOH:H_2O clearly indicate axial ligation with a stronger σ-donor (methanol or water) than observed for $\mathbf{1}^{+}$ in toluene. The ligation of solvent molecule(s) is confirmed by comparison of the ENDOR and HYSCORE spectra of the compounds in normal and deuterated solvents (Figures 6, 7, and S2). An important issue that remains to be addressed is the number of ligating solvent molecules. The appearance of two types of acidic protons in the ENDOR spectra of $\mathbf{1}^{+}$ in methanol suggests a six-coordination for the low-temperature component *D*. DFT computations (Table S2) indicate, however, that the observed difference between the two protons cannot be explained by the difference between the acidic protons of a methanol molecule ligation from the α- or the β-side. Importantly, the DFT computations do not take into account the substitutents on the corrin ring. An NMR analysis of aquocobalamin showed that a hydrogen bond was formed between the cobalt coordinated water molecule and the carbonyl oxygen of the c-acetamide side chain.[75] Such a H-bond can account for the observation of the acidic $H^{(2)}$.

How can we explain the observation of two types of acidic protons in the ENDOR spectra of $\mathbf{1}^{+}$ in MeOH:H_2O in view of the above model? Essentially, two possible explanations can be put forward. In the first, five-coordination with predominantly water ligation from the β-side is taking place, whereby one of the protons is H-bound to the carbonyl oxygen, thus leading to the two distinct acidic protons. The second model involves six-coordination with axial ligation of water or methanol molecules, whereby an acidic proton is H-bound to a carbonyl oxygen along the β-side (but not the α−side). If the latter model would be valid, then we would expect all EPR parameters of $\mathbf{1}^{+}$ in MeOH:H_2O and in methanol at low temperature to be very similar. Instead, drastic differences are observed. The difference in *g* and cobalt hyperfine values observed for $\mathbf{1}^{+}$ in MeOH:H_2O and $\mathbf{1}^{+}$ in methanol (<100 K, component *D*) agrees with the trend expected for an increase of the coordination number (see comparison with data for $Co^{II}(dmgH)_2(H_2O)_2$ [61] or trends observed for ligation of one and two nitrogen bases to Co^{II} porphyrin complexes[77]). Furthermore, the observation that the hyperfine couplings of the corrin nitrogens are similar for $\mathbf{1}^{+}$ in toluene and MeOH:H_2O but decrease for $\mathbf{1}^{+}$ in methanol agrees with DFT predictions for the change from five- to six-coordination (Table 4).

This clearly indicates that for $\mathbf{1}^{+}$ in MeOH:H_2O a five-coordinated complex is found. An important fraction of the population involves ligation of a water molecule from the β-side (observation of two different acidic protons), although it cannot be ruled out that for some complexes methanol is the ligating partner. Indeed, the DFT computations show that the *g* values and the hyperfine couplings with the cobalt nucleus, corrin nitrogens and acidic protons differ only marginally for $\mathbf{3}^{+}$-(MeOH) versus $\mathbf{3}^{+}(H_2O)$ (Table 4, S1, and S2), a difference which will remain undistinguishable in the experiment due to the large observed *g* and *A* strain. The overall spectral analogy between $\mathbf{1}^{+}$ and $\mathbf{2}^{+}$ in MeOH:H_2O indicates that the five-coordination model is also valid for the latter complex.

Finally, we should consider the observed change in the EPR spectrum of $\mathbf{1}^{+}$ in methanol at the methanol phase-transition temperature of 100 K. The similarity between the EPR spectrum of $\mathbf{1}^{+}$ in methanol above 100 K and that of $\mathbf{1}^{+}$ in MeOH:H_2O suggests five-coordination, whereas at lower temperatures six-coordination seems to be dominant. It is known from NMR that there is a large peripheral solvation sphere around B_{12}.[78] The phase transition of methanol will strongly influence this sphere and thus also the structure of the Co^{II} complex. Furthermore, the polar methyl ester substituents of $\mathbf{1}^{+}$ (and also the carboxamide substituents of $\mathbf{2}^{+}$) are likely to take part in the H-bond network formed in the crystalline phase of the solvent. The collapse of this rigid network will make a new coordination situation possible. A preliminary investigation of base-off B_{12r} in methanol[79] also revealed the presence of two components at $T < 100$ K which shows that the observed tendency is not specific for $\mathbf{1}^{+}$. Because at temperatures around 100 K, the solvent molecules are not mobile over larger distances, the sixth solvent molecule must already be in the vicinity of the Co^{II} center, but strong ligation is prevented by the rigid network formed by the solvent molecules and the ring substituents at the α-side of the complex. A collapse of the network allows a

(76) Kräutler, B. In ref 3, p 3.

(77) Walker, F. A. *J. Am. Chem. Soc*. **1970**, *92*, 4235−4244.
(78) Konrat, R.; Tollinger, M.; Kräutler, B. In ref 3, pp 349−361.
(79) Klein, J., personal communication.

sixth solvent molecule to coordinate to Co^{II}. The observation that at $T < 100$ K a small fraction of the molecules is still five-coordinated then probably results from the reduced mobility of the solvent molecules at low temperature. Although the rigid network of H-bonds has been broken up, only part of the solvent molecules can actually coordinate to the cobalt(II) ion.

X-ray absorption spectroscopic studies suggest that at room-temperature chemically induced free *base-off* B_{12r} is six-coordinated to water,[22] whereas electrochemically formed *base-off* B_{12r} has been deduced to be five-coordinated.[21] The basis for this difference is difficult to interpret. Geometry optimization studies using DFT indicate that Co^{II} corrins can bind one or two axial water, with relatively long bond lengths in the six-coordinate form ($\mathbf{3}^+(H_2O)$: $r(Co-O) = 0.234$ nm; $\mathbf{3}^+(H_2O)_2$: $r(Co-O)_\beta = 0.250$ nm, $r(Co-O)_\alpha = 0.261$ nm). The discovery of 6-coordinate Co(II)corrins, for which the axial bonds have been calculated to be considerably longer than those in corresponding 5-coordinate forms is of interest with respect to the finding of "long" axial bonds in several crystal structures of corrinoid proteins.[11,12] Careful analysis of the effect of X-ray irradiation on protein crystals with corrinoid cofactors has revealed the likelihood of inadverted radiation induced reduction to (hexa-coordinate) Co(II)corrinoids.[80] The calculated difference in the Co−O bond length between the α- and β-side is interesting and perhaps lies at the basis of the apparently contradicting XAS results.

Furthermore, the large similarity in the spectra of $\mathbf{1}^+$ and $\mathbf{2}^+$ in MeOH:H_2O confirms that $\mathbf{1}^+$ is an adequate model system for *base-off* B_{12r}. For many years, bis(dimethylglyoximato) cobalt ($Co^{II}(dmgH)_2$) complexes have been extensively studied as cobalamin models.[5a,81] However, comparison of the *g* and cobalt hyperfine values (Table 1) and the hyperfine and nuclear quadrupole data of the equatorial nitrogens (Table 2) of $\mathbf{2}^+$ and $Co^{II}(dmgH)_2$ indicates that the electronic structure of the latter complex differs considerably from the one of *base-off* B_{12r}, which will inevitably have a large influence on the chemical activity.

The combination of ENDOR experiments and DFT computations also revealed that the hyperfine interaction of the corrin proton H19 is clearly distinguishable from the other protons. Our analyses now show that this proton carries the largest spin density of all protons in the corrin ring; indeed, the bond H−C(19) is oriented roughly along the *z*-axis and parallel to the p-orbitals of the corrin π-system, providing good orbital overlap. It is interesting to note also, that an important step in the B_{12}-biosynthesis involves the reduction of the C18−C19 double bond in precorrin-6A. NMR in combination with selective deuteration of NADPH showed that the C19 center receives the hydride equivalent from NADPH.[82]

Finally, Table 2 shows that the ring nitrogens are very sensitive to structural changes. The coordination of one versus two axial ligands is reflected by the anisotropy of the hyperfine interaction. Furthermore, the nuclear quadrupole interaction senses the difference in the ring structure. The values of $|e^2qQ/h|$ for the corrin and porphyrin nitrogens are similar, whereas they almost double for the nitrogens of the chemically distinctive dimethylglyoximato ligand. The asymmetry parameter η is clearly different for the corrin and porphyrin ligands. This parameter reflects the deviation of the electric field at the nitrogens from cylindrical symmetry and depends on the total electron density, which differs for the two ligands.

Conclusion

The present EPR-study on the Co(II)corrrins Cob(II)ester ($\mathbf{1}^+$) and base-off B_{12r} ($\mathbf{2}^+$) provides the first direct evidence for axial solvent ligation in polar solvents. Indeed, no evidence of pure four-coordinated Co^{II} corrins in solution is found. This is important in view of the fact that base-off cobalt(II) corrinates are sometimes suggested as being four-coordinated.[4,22] In methanol, the axial ligation of $\mathbf{1}^+$ is temperature dependent and correlates with the phase transition of the solvent. A penta-coordinate Co(II)-center with axial ligation of one methanol molecule is observed in the α-crystalline phase, whereas six-coordination becomes possible in the glassy state. The relation to the phase transition could be established by different cooling experiments and by the use of a H_2O:methanol mixture. Addition of water to methanol changes its phase-transition properties and leads to frozen solutions with a large degree of crystalline structure even at low temperature. In this solvent mixture, $\mathbf{1}^+$ occurs only in the five-coordinated form. Differences in the solvent ligation are related to changes in the network formed by the solvent molecules and the ring substituents. In apolar solvents $\mathbf{1}^+$ forms a contact-ion pair with its counterion, perchlorate. In the crystal,[7] the perchlorate ion is bound as axial ligand to the Co(II)-center.

Our investigation shows that EPR forms an excellent tool to analyze subtle changes in the electronic structure of Co^{II}-corrin systems, especially when they are supported by DFT computations. Furthermore, our study shows that the solvent and the phase-transition properties of the solvents can have a large influence on the structure (and consequently the EPR data) of metal complexes. This can be important in cases where smaller complexes are studied as models for cofactors in a protein. It is to be expected that the influence of the freezing characteristics of the solvent will be less severe in a protein-embedded cofactor, so that wrong conclusions might be drawn from comparison with the model system

Acknowledgment. This research has been supported by the Swiss National Science Foundation and by an exchange program between the Weizmann Institute in Israel and ETH Zurich (Switzerland).

Supporting Information Available: Simulation of A and Q strain effects in HYSCORE; difference-HYSCORE spectra of $\mathbf{1}^+$ in CD_3OD and in CH_3OH, of $\mathbf{1}^+$ in CD_3OH and in CH_3OH, and of $\mathbf{1}^+$ in CD_3OD and in CD_3OH; computed *g* and cobalt hyperfine values for the different types of axial ligation to $\mathbf{3}^+$ and computed hyperfine (nuclear quadrupole) values of the solvent protons (deuterium nuclei) of different Co^{II} corrin complexes. This material is available free from charge via the Internet at http://pubs.acs.org.

JA021218J

(80) Champloy, F.; Gruber, K.; Jogl, G.; Kratky, C. *J. Synchrotron Rad.* **2000**, *7*, 267−273.
(81) Wirt, M. D.; Bender, J. C.; Peisach, J. *Inorg. Chem.* **1995**, *34*, 1663−1667.
(82) Weaver, G. W.; Leeper, F. J.; Battersby, A. R.; Blanche, F.; Thibaut, D.; Debussche, J. *Chem. Soc., Chem. Commun.* **1991**, 976−979.